ACSNANO

www.acsnano.org

ARTICLE

Light-Programmable Logic-in-Memory in 2D Semiconductors Enabled by Supramolecular Functionalization: Photoresponsive Collective Effect of Aligned Molecular Dipoles

Ye Wang, Daniel Iglesias, Sai Manoj Gali, David Beljonne, and Paolo Samorì*

Cite This: *ACS Nano* 2021, 15, 13732–13741

Read Online

ACCESS | Metrics & More | Article Recommendations | Supporting Information

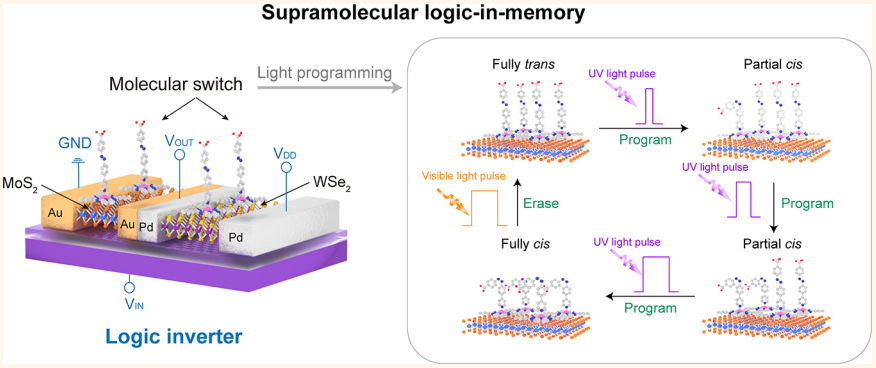

ABSTRACT: **Nowadays, the unrelenting growth of the digital universe calls for radically novel strategies for data processing and storage. An extremely promising and powerful approach relies on the development of logic-in-memory (LiM) devices through the use of floating gate and ferroelectric technologies to write and erase data in a memory operating as a logic gate driven by electrical bias. In this work, we report an alternative approach to realize the logic-in-memory based on two-dimensional (2D) transition metal dichalcogenides (TMDs) where multiple memorized logic output states have been established via the interface with responsive molecular dipoles arranged in supramolecular arrays. The collective dynamic molecular dipole changes of the axial ligand coordinated onto self-assembled metal phthalocyanine nanostructures on the surface of 2D TMD enables large reversible modulation of the Fermi level of both *n*-type molybdenum disulfide (MoS_2) and *p*-type tungsten diselenide (WSe_2) field-effect transistors (FETs), to achieve multiple memory states by programming and erasing with ultraviolet (UV) and with visible light, respectively. As a result, logic-in-memory devices were built up with our supramolecular layer/2D TMD architecture where the output logic is encoded by the motion of the molecular dipoles. Our strategy relying on the dynamic control of the 2D electronics by harnessing the functions of molecular-dipole-induced memory in a supramolecular hybrid layer represents a versatile way to integrate the functional programmability of molecular science into the next generation nanoelectronics.**

KEYWORDS: *two-dimensional material, molecular switch, azobenzene, transition metal dichalcogenides, logic-in-memory, supramolecular chemistry*

Information technologies, with their exponentially increasing demand of data manipulation, require a colossal number of computer units to fulfill efficient data processing and storage. The prevailing von Neumann architecture in computers is reaching a bottleneck where the computing and memory units are physically separated increasing the concerns for energy efficiency. Therefore, the in-memory computing is being optimized in order to meet the

Received: June 17, 2021
Accepted: August 4, 2021
Published: August 9, 2021

https://doi.org/10.1021/acsnano.1c05167
ACS Nano 2021, 15, 13732–13741

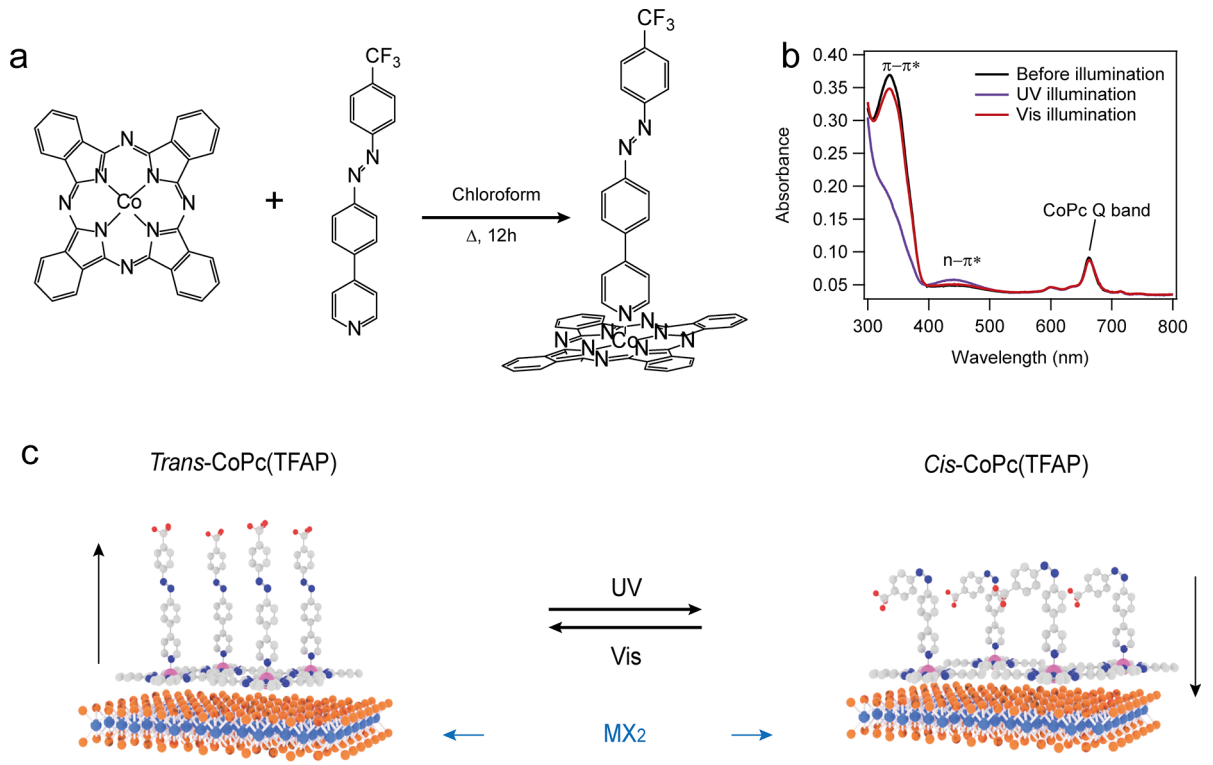

Figure 1. Light-induced motion of the molecular switch on the 2D surface. (a) Coordination of CoPc and the photoswitchable TFAP ligand. (b) UV–vis spectra of the photoswitchable of the CoPc(TFAP) complex in chloroform. (c) Scheme of the *trans* and *cis* state molecular switch on MX_2 (M = Mo, W; and X = S, Se) surface controlled by light.

present requirements.[1−3] The engineering concept of logic-in-memory (LIM) devices relies on the incorporation of non-volatile memory units, *e.g.*, floating gate and ferroelectric gate, in metal-oxide-semiconductor field-effect transistor (MOSFET) based logic gates.[4,5] In these devices, either by charging−discharging or by electrical polarization, data are stored in the logic memory by electrically manipulating the control gate, thereby modifying the magnitude of the current passing through the channel. While the electrical control for operating logic gates to impart memory functions is efficient, other approaches for memory writing and reading, such as those driven by optical stimuli, are also necessary to add functional diversification in logic-in-memory computing, in particular, in extreme circumstances where optoelectronic memory is more facile to access.

One of the best solutions to achieve such a goal is to realize optically controlled memory devices by using photochromic molecular switches.[6−11] The light-induced isomerization in photochromes can be used not only to amplify the functionality of materials in the form of work function tuning and reversible doping, but also to allow such molecular switches to operate as active elements in memory manipulation.[10,12−17] Common photochromic molecules include azobenzene, diarylethenes, stilbene, spiropyrans, and their derivatives. The simple chemical structures of the molecules make them convenient for blending or chemically grafting on organic/polymer semiconductors, ensuring robust functionalization. Two-dimensional (2D) materials are a better "partner" for the molecular switches, in view of their extraordinary physical and chemical properties.[18,19] Among them, transition metal dichalcogenides (TMDs) are the most studied semiconducting 2D materials with a layer-dependent bandgap and high field-effect mobility and I_{on}/I_{off} ratio. The variety of electronic properties of the TMD family makes them suitable components for building up *n*-MOSFET and *p*-MOSFET, which are key elements of binary logic devices. A number of organic molecules could be stably physisorbed on the atomically thin, ultraflat surface 2D TMDs by $\pi-\pi$ stacking, therefore inducing striking influences such as doping, forming van der Waals (vdW) heterostructures and so forth.[20,21] The most representative photochromic molecule, *i.e.*, azobenzene, has been used to functionalize graphene and MoS_2 leading to improved exfoliation, enhanced photoresponse and light-controlled doping, emission tuning, *etc.*[22−27] In particular, the reversible dipole-induced doping effect of azobenzene photoswitches, which modulates the threshold voltages and channel current dynamically by light stimuli, makes it an ideal system to establish optoelectronic memory on 2D logic devices.

Azobenzene molecules have been tethered to the surface of 2D materials either covalently or non-covalently. In the former case, the functionalization unfortunately displays a low yield as a result of the limited reactivity of 2D materials with organic species. In the latter case, the azobenzenes are closely packed lying flat on the 2D surface, with the photoisomerization yield to some extent limited by steric hindrance. Moreover, within the films the dipoles display a moderate degree of structural order. As a result, the light-triggered magnitude of dipolar change at the ensemble level is not enough to ensure a large optoelectronic memory window on the 2D devices. An alternative strategy consists of using a molecular platform as a base with an anchoring point to control the patterning, thus positioning, of azobenzenes by placing them at ca. 1 nm far apart adopting an upstanding conformation.[21,28−30] More

https://doi.org/10.1021/acsnano.1c05167
ACS Nano 2021, 15, 13732−13741

precisely, the distance between two adjacent azobenzenes is dictated by the lateral size of the platform, which is always much larger than the cross section occupied by an up-standing azobenzene; thus, the motion of azobenzenes is not sterically hindered by the adjacent photochromes and the photoswitching is expected to take place with a relatively high yield. Furthermore, if the vertically aligned azobenzenes all display the same orientation forming periodic structures, the photoswitching can be characterized by collective effects. The latter would enable maximization of the influence on the electronic properties of 2D materials underneath. Several previous works showed that triazatriangulenium (TATA) ions on the surface could be an appropriate platform to bind azobenzene with ethinyl or phenyl spacers where the photoisomerization of freestanding azobenzene is observed by scanning tunneling microscopy (STM).[28,31,32] Recently, this class of molecule has been proven to enhance Raman signals and modulate the work functions of 2D materials.[33,34] However, production of the TATA platform requires a multistep cumbersome synthesis, whereas a thermodynamically driven approach based on molecular self-assembly would be more convenient. Among others, metal porphyrins and phthalocyanines are well-established molecular scaffolds that are usually flatly physisorbed on 2D materials and could also provide such functionality for growing axially bonded azobenzene ligands in a more versatile and modular manner.[35−38] As we have previously demonstrated, the axial coordination of metal and functional pyridines is a viable route to generate a vertical electrical field to monolayer MoS_2 thanks to different alignments and magnitudes of molecular dipoles (taking advantage of the confinement of crystal field of octahedral transition metal d-orbital of zinc and cobalt phthalocyanine).[21,39−41] The method has also been proven recently for stable growth of larger π-conjugated pyridinic ligands.[42] Our previous observations revealed that the dipole-induced doping of axially coordinated pyridines could attain $10^{12}/cm^2$ of the charge carrier density change to MoS_2, being comparable to traditional electron donor/acceptor molecules, ensuring a memory window of more than 20 V on SiO_2 dielectric. Azobenzene molecules, whose molecular dipole could easily be tuned by photoisomerization, represent the best candidate for achieving collective dynamic doping on 2D materials. Therefore, in this work, we target the design of a molecular switch in which the azobenzene ligand is oriented perpendicular to the 2D surface. The molecular platform is used to template the azobenzene growth enabling the precise construction of optoelectronic memory of 2D logic devices operating through the collective effect of molecular dipoles that are controlled by light.

RESULTS

Our designed molecular switch is composed of a macromolecular metal complex, cobalt phthalocyanine, and a pyridinic ligand containing azobenzene (4-(4-((4-(trifluoromethyl)phenyl)diazenyl)phenyl)pyridine, denoted as TFAP; for synthetic details see Methods and Supporting Note 1 (Figure S1−S3) in Supporting Information) as the light-responsive unit (Figure 1a). The UV−vis absorption spectrum in chloroform shows the expected features for azobenzene derivatives with an intense band at 355 nm and broad low-intensity band at 455 nm attributed to the $\pi-\pi^*$ and $n-\pi^*$, respectively (Figure S4c). Ultraperformance liquid chromatography coupled to high-resolution mass spectrometry (UPLC-HRMS) measurement revealed that the starting isomer is approaching 100% *trans*-TFAP (Figure S4b). The *trans* to *cis* photoisomerization of TFAP was studied upon irradiation of a diluted solution with a UV LED lamp (λ_{max} = 367 nm, 2.4 mW cm^{-2}). Figure S4a displays the variations of the light absorption due to the gradual transformation of the *trans* to the *cis* isomer. Notably, the band at 355 nm decreased, while the band at 455 nm increased. Under the explored experimental conditions, the photostationary (UV-PSS) state was reached after 12 min of irradiation. Then, the back isomerization to the *trans* isomer was fully achieved upon irradiation with a visible LED lamp (λ_{max} = 451 nm, 2.1 mW cm^{-2}). The photoswitching behavior of the axial coordinated complex of the TFAP ligand and CoPc (denoted as CoPc(TFAP)) is demonstrated in Figure 1b where both the Q band (630−700 nm) and B band (300−400 nm) of CoPc and the $\pi-\pi^*$ band TFAP (350 nm) are presented with an association constant of 5857 and 5941 M^{-1} in chloroform and DMSO, respectively (for detailed titration spectra, see Supporting Note 2 in the Supporting Information). Similar to the photoswitching of TFAP, the $\pi-\pi^*$ band decreased and $n-\pi^*$ (455 nm) increased upon UV irradiation, and the absorption was recovered by irradiation with visible light. Time-dependent photoswitching is demonstrated in Figures S7−S8 in the Supporting Information. Due to the overlap of the B band of CoPc and the $\pi-\pi^*$ band of TFAP (which is in accordance with the literature[43,44]), even at the photostationary state of both V_{th} shifts, a weak absorption at 300−400 nm has been observed. The Q-band turned out to be unaffected by the photoisomerization of TFAP, indicating the absence of electronic coupling between the two chromophores (Figure S8, Supporting Information).[43,45]

The complex photoswitching element at the *trans* conformation intrinsically possesses a large molecular dipole moment whose magnitude is to a great extent determined by the strong electron-withdrawing property of the $-CF_3$ group at the extremity of the TFAP ligand. The photoisomerization of the complex triggers the rotation/inversion of N═N−C bond. The $-CF_3$ group is therefore brought closer to the 2D surface yielding to a shift of the molecular dipole direction (Figure 1c). The modulation of the functional group distance and orientation brings a distinct and collective change of the molecular dipole from +3.55 D (pointing out of the basal plane of MX_2) to −1.40 D (pointing toward the basal plane of MX_2) for MoS_2 and from +3.42 D to −1.58 D for WSe_2, as shown in Figure 1c. Such large molecular dipoles act as a local electrical gate to atomically thin 2D material, introducing a decrease of the work function of MX_2 from 5.31 to 5.07 eV for MoS_2, and from 4.66 to 4.27 eV for WSe_2, as demonstrated in detail in the DFT calculations in Figures S9−S10, Supporting Information. The shift of the work function could directly influence the drain−source current (I_{ds}) of the MOSFETs based on 2D MX_2, hence realizing the program−read−erase process of the memory cell dynamically as driven by external light stimuli. Here, we demonstrate how the isomerization of the azobenzene could establish a memorized electrical output in the field-effect transistors (FETs) of both *n*-MOSFET and *p*-*MO*-SFET of 2D TMDs, and be applied in a light-programmable logic-in-memory NOR gate based on these 2D MOSFET, thus realizing a dynamic electrical switch without fabricating complex circuitries.

Before elucidating how molecular switches could serve as optoelectronic memory units of binary inverters, we *first*

https://doi.org/10.1021/acsnano.1c05167
ACS Nano 2021, 15, 13732−13741

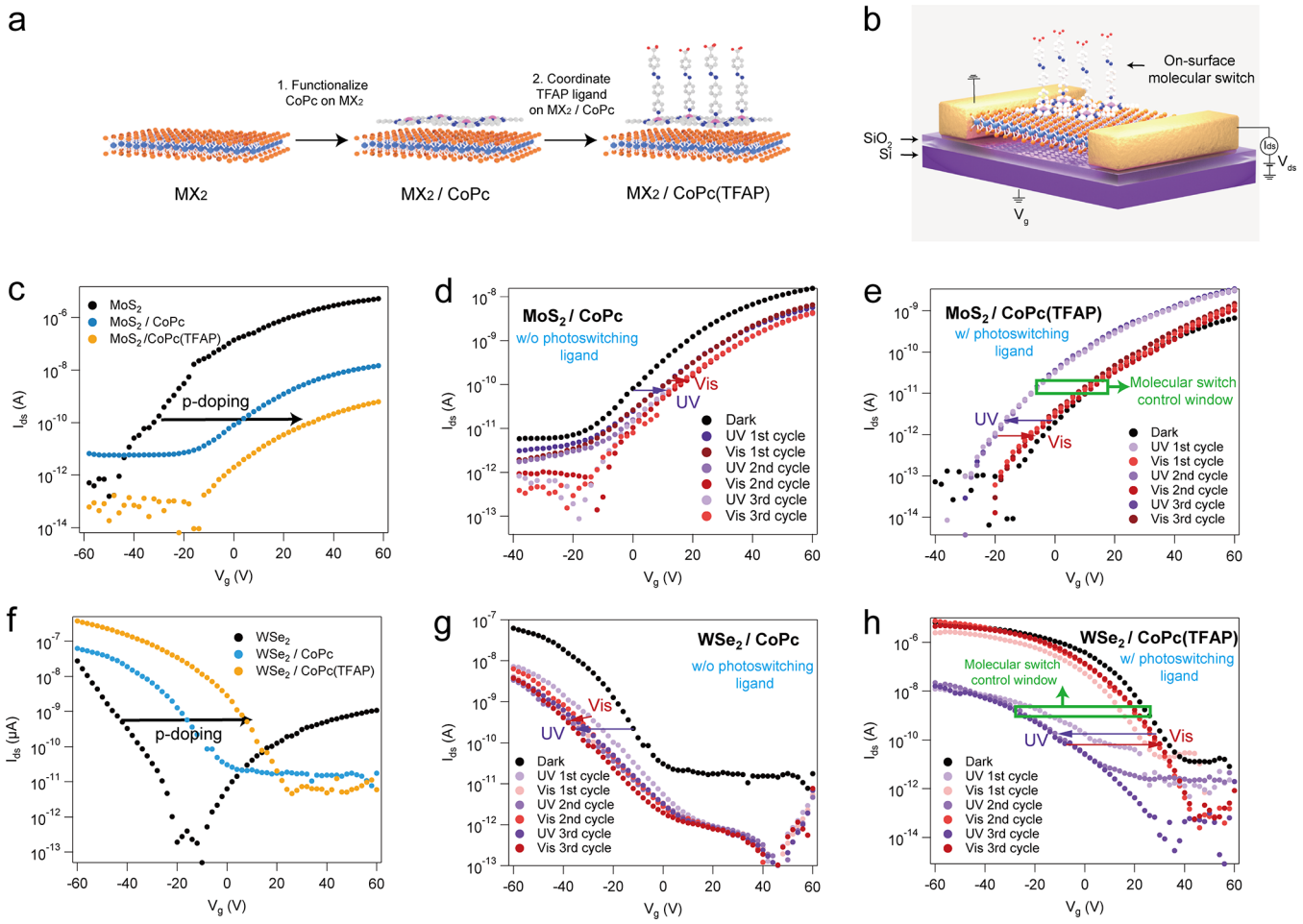

Figure 2. Molecular switch control over dynamic doping of MX_2 FET. (a) On-surface growth of molecular switch. (b) Device structure of MX_2 FET controlled by molecular switch. (c) I_d–V_g curve of MoS_2 FET before and after each step of molecular switch growth. (d,e) Photoswitching of the molecular switch on MoS_2 (d) before and (e) after the coordination with TFAP ligand. (f) I_d–V_g curve of WSe_2 FET before and after each step of molecular switch growth. The doping from the CoPc(TFAP) complex leads to pure p-type transport in WSe_2, compared to the ambipolar characteristics in the initial state. (g,h) Photoswitching of the molecular switch on WSe_2 (g) before and (h) after coordination with the TFAP ligand.

evaluated the influence on the building blocks of binary inverters: n- and p-type MOS (NMOS and PMOS). Here, we used monolayer MoS_2 and few-layer WSe_2 as NFET and PFET. Previous works from our group showed that optically tunable molecular dipole enables one to reversibly dope 2D TMDs by using light as a remote control.[26,46−48] Inspired by these findings, we exploit our molecular switch as a dynamic doping remote control for MoS_2 and WSe_2 based transistors. We adopt the two-step on-surface axial ligand growth strategy from our previous work which is critical for guaranteeing a maximized collective dipole growth out of the plane of 2D MX_2 (detailed information, see Figure S11), as illustrated in Figure 2a.[21] Unlike traditional approaches in the decoration of 2D materials with azobenzene switches which suffer from incomplete photoswitching due to the dense packing on the surface, the TFAP ligand in the complex is freestanding with a large degree of conformational freedom for switching from the *trans* to *cis* isomer thanks to the large planar molecular area and spacing dictated by the CoPc platform.[31,49−51] Such an edge-on geometry of the azobenzenes is also particularly suitable to manipulate the molecular dipoles in the direction perpendicular to the basal plane of the TMD surfaces, which was proven to be the best orientation to boost the doping effect.[46,47] AFM images (Figure S12 in the Supporting Information) and XPS spectra (Figure S13 in the Supporting Information) provide evidence for the efficient coordination of the TFAP ligand after the second step of functionalization. The resulting molecular-switch-functionalized MX_2 MOSFET is depicted in Figure 2b. A distinct p-doping is observed after each step of functionalization with a final charge carrier density shift of $4.38 \times 10^{12}/cm^2$ for MoS_2 and $2.40 \times 10^{12}/cm^2$ for WSe_2 (Figure 2c and f). In order to distinguish the doping caused by the light-induced charge transfer between CoPc and MX_2, and the doping from the photoswitching between the two states of the molecular switch, we conducted UV and vis switching cycles for both MX_2/CoPc heterostructures with and without the TFAP ligand. As demonstrated in Figure 2d, the illumination by UV light induced a slight p-doping to MoS_2, corresponding to electron transfer from the conduction band of MoS_2 (4.1 eV) to the first reduction potential of CoPc (4.31 eV), while by illuminating with visible light, the electron transfer was not recovered through the cycles. Conversely, for WSe_2, with the major charge carrier being a hole, we observed a slight irreversible photoinduced hole transfer from the valence band of WSe_2 (4.8 eV) to the first oxidation state of CoPc (5.5 eV) (Figure 2g and Figure S14, Supporting

https://doi.org/10.1021/acsnano.1c05167
ACS Nano 2021, 15, 13732−13741

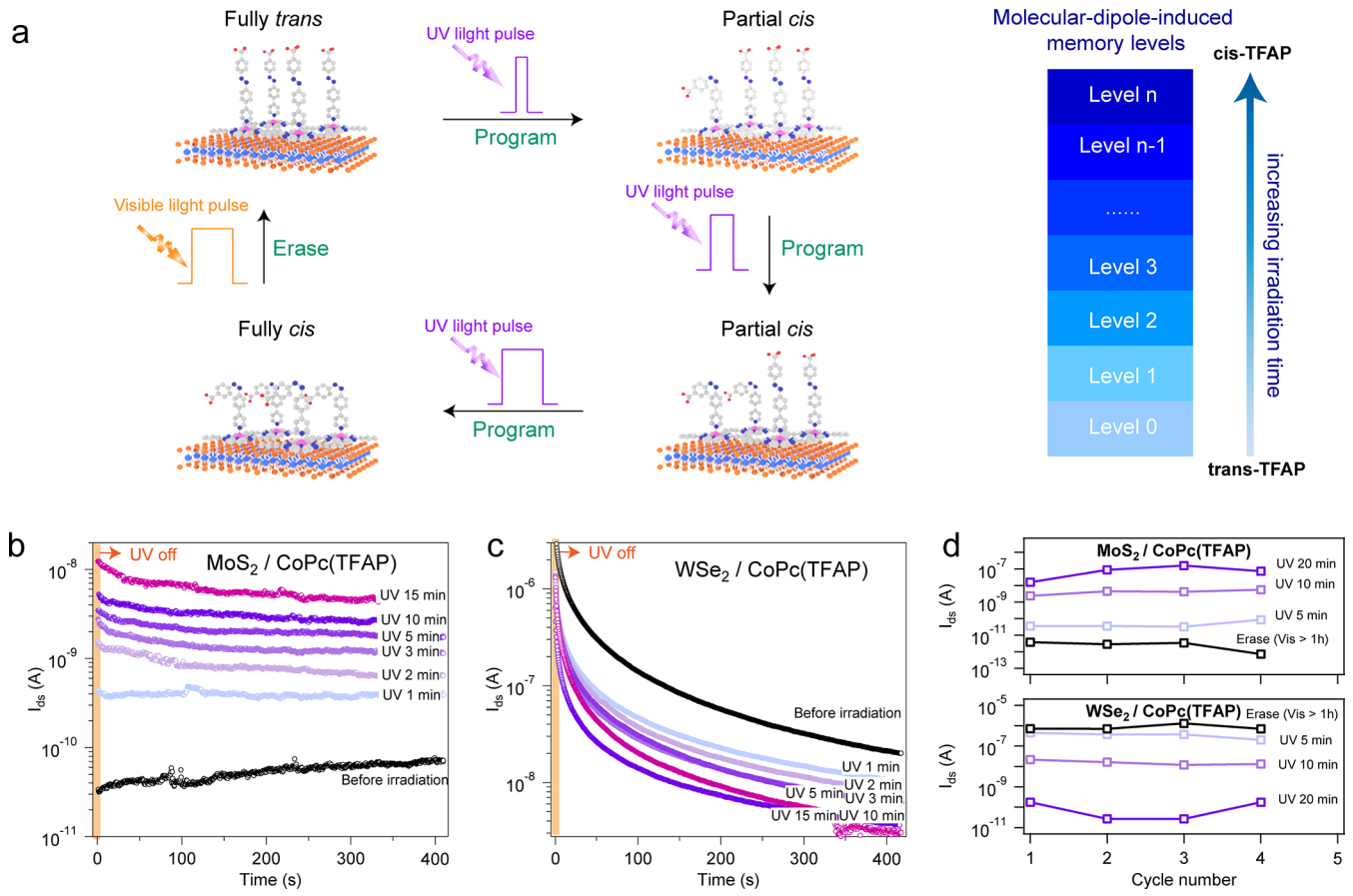

Figure 3. Time-dependent light programming and reliability of the photoswitching ligand on MoS_2 and WSe_2 FETs. (a) Schematic representation of the program−erase process by light pulses and multilevel control of memory states by axial photoswitching ligands. (b,c) Retention curves of (b) *n*-type MoS_2 (V_g = 0 V, V_{ds} = 1 V) and (c) p-type WSe_2 (V_g = −60 V, V_{ds} = 1 V) with various UV switching time. (d) Channel current within program and erase cycles.

Information). After adding the photoswitching ligand TFAP on MX_2/CoPc, as shown in Figure 2e and h, the light irradiation of the on-surface molecular switches determined a dynamic doping control window of on average $(1.18 \pm 0.79) \times 10^{12}/cm^2$ for MoS_2 and $(2.18 \pm 0.15) \times 10^{12}/cm^2$ for WSe_2 (statistical analysis, see Figure S15 in the Supporting Information).

The change in the orientation of the dipole moment upon isomerization from the *trans* state to the *cis* form occurring on an Avogadro number of molecules gives rise to a collective effect which is reflected in the major threshold voltage (V_{th}) shift upon light irradiation. The photoconductive and persistent photocurrent effects of MX_2 on the SiO_2 dielectric are ruled out in our experiments, as demonstrated in control experiments carried out by fabricating graphene MOSFET which has no photoconductive effect due to the zero bandgap (Figures S16−S17, Supporting Information). Furthermore, we have observed an opposite V_{th} shift with a pure TFAP ligand randomly physisorbed on the surface without any special confinement (Figure S18, Supporting Information). The molecular switch controlled dynamic doping is also reflected in the optical properties of MoS_2, as discussed in Figure S19 in Supporting Information. By and large, by remotely controlling with light the isomerization of the azobenzenes, one can fabricate transistors featuring a dynamic threshold voltage, which is beneficial for applications in smart electronics. According to the time-dependent photoswitching of the TFAP ligand, the stepwise modulation of the work function of MX_2 could be achieved by alternating the photoswitching time. As demonstrated in Figure 3a, multiple intermediate states between the initial (denoted as "fully *trans* state") and the photostationary state (denoted as "fully *cis* state") can be reached. Therefore, we could realize the programming of the memory current by UV light with different irradiation times with the CoPc(TFAP) serving as a light-triggered "floating gate". In Figure 3b, we track the time-dependent channel current at V_g = 0 V of MoS_2 FET. The initial I_{ds} is in the 10^{-11} A scale, denoting the OFF state of the transistor. Upon illumination for 1 min with UV light, the partial switching of the TFAP ligand determines a negative shift of the threshold voltage and gives rise to an increase of the I_{ds} to 10^{-10} A. Upon longer irradiation times, the I_{ds} further increases up to 10^{-8} A, demonstrating an extinction ratio of 10^3. More precisely, it was possible to define 5 intermediate memory states programmed by 1, 2, 3, 5, and 10 min. Conversely, as hole transport is dominant in WSe_2 FET, a decrease of the channel current with the same UV light programming strategy was observed due to the negative shift of the threshold voltage (Figure 3c). The programmed memory current reaches the value of 10^{-9} A at V_g = −60 V compared to 10^{-7} A at the initial state, showing an extinction ratio of 10^2, hence being comparable to optoelectronic memories based on traditional floating gate technologies.[52] The erase process could be accomplished by irradiating the FETs by visible light, thus upon switching the TFAP from

https://doi.org/10.1021/acsnano.1c05167
ACS Nano 2021, 15, 13732−13741

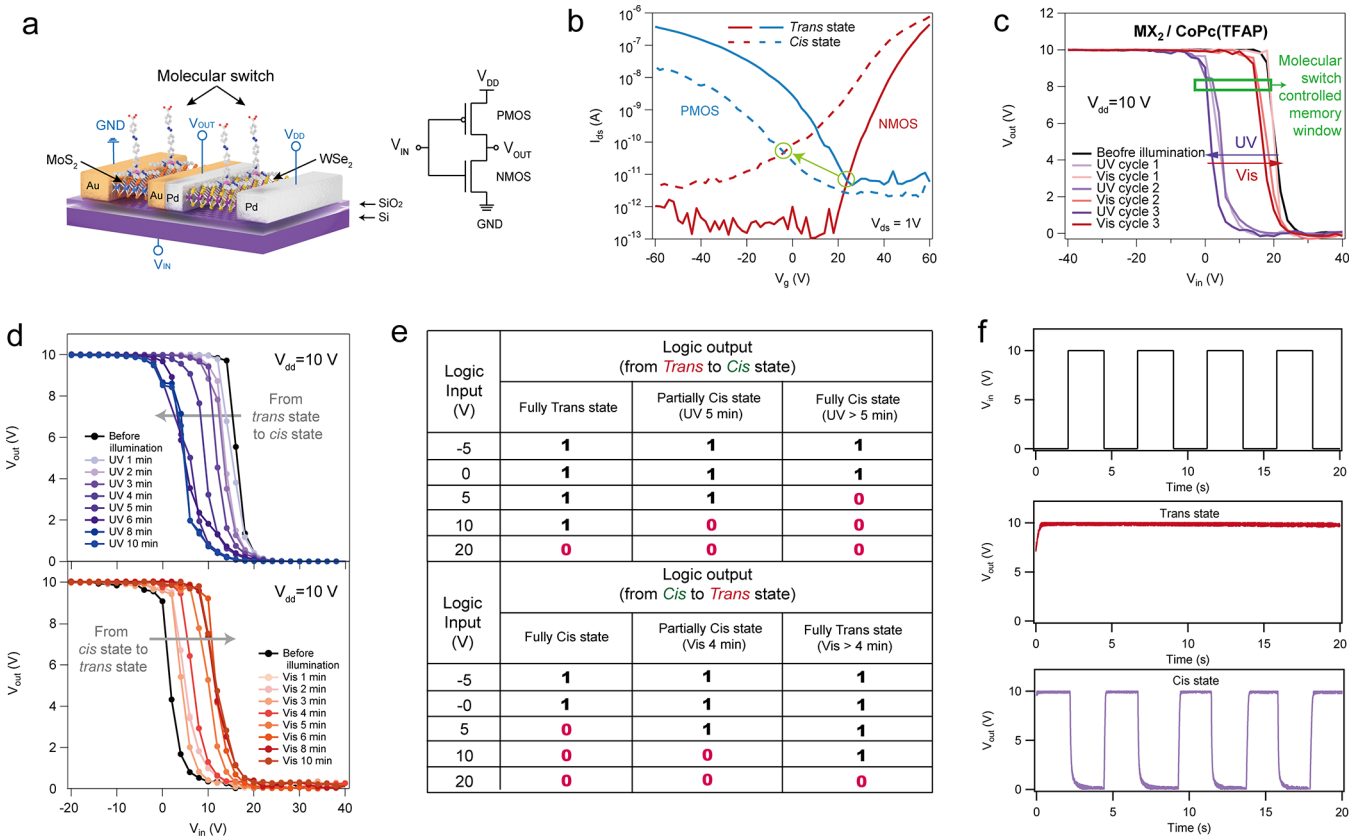

Logic Input (V)	Logic output (from *Trans* to *Cis* state)		
	Fully Trans state	Partially Cis state (UV 5 min)	Fully Cis state (UV > 5 min)
-5	1	1	1
0	1	1	1
5	1	1	0
10	1	0	0
20	0	0	0

Logic Input (V)	Logic output (from *Cis* to *Trans* state)		
	Fully Cis state	Partially Cis state (Vis 4 min)	Fully Trans state (Vis > 4 min)
-5	1	1	1
-0	1	1	1
5	0	1	1
10	0	0	1
20	0	0	0

Figure 4. Molecular switch enabled a light-programmable logic-in-memory device. (a) Schematic representation and the circuit of the molecular switch controlled MoS_2−WSe_2 binary inverter. (b) Transfer characteristics of the n- and p-MOSFET with the molecular switch on both *trans* state and *cis* state. (c) V_{out}−V_{in} of the inverter and the dynamic cycles controlled by the molecular switch. The green circle indicates two distinctive transition points from different switch states. (d) V_{out}−V_{in} of the programmable dynamic switching point transition of the inverter controlled by illumination time on molecular switch. (e) Summary of the programmable dynamic logic output states by manipulating the molecular switch motion with UV and vis illumination time. The measurement is done at V_{dd} = 10 V. The logic output "1" corresponds to V_{out} = 10 V and logic output "0" corresponds to V_{out} = 0 V. (f) Time-dependent V_{out} of the inverter with V_{in} pulse cycles at *trans* and *cis* states of the molecular switch showing distinct output signals in the two states. The *cis* state (metastable state) of molecular switch shows stability over the gate electrical field.

the *cis* back to the *trans* isomer. The photoswitching could also endure several program−erase cycles, as shown in Figure 3d.

Based on previous discussions, our on-surface molecular switches could achieve dynamic control of threshold voltages by building an optoelectronic memory window on transistors of both MoS_2 and WSe_2. It is essential to explore how they perform when these molecular-switch-controlled devices are embedded in electronic circuits. While the demand of data storage and simultaneous fast computing has been rising dramatically in recent years, logic-in-memory holds the potential to become an important solution to energy-efficient computing for semiconductor industry. To address this challenge, we have built up a binary logic inverter (NOR gate) in which the MoS_2 and WSe_2 MOSFETs are in series in order to demonstrate a logic-in-memory device realized by molecular switches. The architecture and the electrical circuit and the optical microscope image of the inverter are displayed in Figure 4a and Figure S20a in the Supporting Information. Each MOSFET (NMOS being MoS_2 channel and PMOS being WSe_2 channel) exhibited unipolar transfer characteristics with $I_{on}/I_{off} > 10^5$ (Figure 4b) and both of their V_{th}'s shift negatively at the *cis* state compared to the *trans* state. The V_{out} versus V_{in} of the inverter is presented in Figure 4c together with the gain shown in Figure S20b in Supporting Information. The large dipolar doping from the *trans* conformation of the molecular switch gave rise to the transition point appearing in the range of +18 V to +20 V, showing highly skewed inverter characteristics. While triggering the isomerization to the *cis* form, we could successfully adjust the transition point at $V_{dd}/2$ (5 V), reaching the critical performance of an ideal inverter. This shift of the inverter transition point was found to be fully reversible through UV−vis illumination cycles, creating a memory window of 20 V. Here, the molecular switch could be considered a light-programmable "molecular switch floating gate" in which the readout of the inverter underneath could be programmed and erased upon irradiation at different wavelengths. The existence of the memory window of the inverter can be attributed uniquely to the motion of the azobenzene unit on the TFAP ligand in the molecular switch. Conversely, in the absence of the ligand, the inverter showed a static transition point even with long illumination time (Figure S21, Supporting Information). The shift was also found to be time-dependent, according to the molecular kinetics of the TFAP ligand.

As demonstrated in Figure 4d, the illumination time on the molecular switch was critical to the logic output such that for the same V_{in}, V_{out} could be different according to the configuration of the molecular switch on surface. In this

https://doi.org/10.1021/acsnano.1c05167
ACS Nano 2021, 15, 13732−13741

case, we realized a programmable logic device prototype by modulating the motion state of molecular switch, hence achieving dynamic logic output by UV−vis illumination. By taking advantage of the azobenzene isomerization, we could define three programmable memory states of the inverter where the molecular switch is at (1) *fully trans* state, (2) *partially cis* state, and (3) *fully cis* state. The logic output results are listed in Figure 4e where the molecular switch state programming generates different logic output values for the same input voltage, which are reversible by changing the illumination wavelength. Furthermore, the programmable dynamic logic output could be maintained through input pulse cycles (Figure 4f) on a long time scale and is reproducible among different devices (Figure S22, Supporting Information), hence realizing the logic-in-memory manipulation. More importantly, our fabrication process is less complex and expensive, and features improved tunability thanks to the broadest arsenal of molecular structure switches available.[4,53]

CONCLUSION

In summary, we have demonstrated an original and modular concept to exploit on-surface molecular switching events to modulate the electronics of 2D semiconductors. The use of a molecular platform to place light-responsive molecules at a 1 nm distance with a controlled orientation of the molecular dipoles perpendicular to the surface enabled to make full use of the photoisomerization of azobenzene switches to maximize the reversible doping of 2D semiconductors. Such a dynamic strong doping modulation has paramount importance for field-effect transistor applications and most importantly also to establish a multistate reversible memory current enabled by light stimuli at specific wavelengths. Finally, the integration of molecular switches on logic circuits made it possible to implement light-programmable dynamic logic output simply by tuning the light illumination, thereby realizing an unparalleled prototype of logic-in-memory devices. These findings provide unambiguous evidence for the power and versatility of molecular switches when interfaced with 2D materials to accomplish advanced electronic functions, offering a non-conventional solution for the next generation of remotely controlled of (nano)devices.

METHODS

Sample Preparation. Monolayer MoS_2, few-layer WSe_2, and graphene were mechanically exfoliated from commercially available crystals (Furuchi, Japan for MoS_2; HQ graphene for WSe_2; Materials Quartz, Inc. for HOPG) using the Scotch tape method and transferred on thermally oxidized heavily n-doped silicon substrates (Fraunhofer Institute IPMS, ρSi ∼ 0.001 Ω·cm, t^{ox} = 270 nm). Their thickness was monitored by optical microscopy combined with Raman spectroscopy and atomic force microscopy (AFM). The samples were thermally annealed at 200 °C inside a vacuum chamber to desorb atmospheric adsorbates. CoPc are purchased from Merck. The MX_2/CoPc hybrids were realized by immersing monolayer MoS_2 into 0.5 mM CoPc in DMSO solution for 10 min to attain a high coverage of molecule without degrading the electrical performances of the heterostructure (Figure S23 in the Supporting Information), and then rinsed vastly with chloroform, acetone, and IPA and thermally annealed in nitrogen to remove aggregates and evaporate solvents. To avoid the desorption of MPc on MX_2 when reacting with ligands in a solvent environment, chloroform (which does not dissolve CoPc) was chosen to be the solvent for the azopyridinic ligand. The MX_2/MPc heterostructures on Si/SiO_2 substrate were directly immersed in a ligand solution at 40 °C for 12 h followed by rinsing vastly with chloroform, acetone, and IPA and thermal annealing in nitrogen. The functionalized samples are measured after being cooled to room temperature.

Synthesis of Photoswitchable Ligand. 4-(4-((4-(Trifluoromethyl)phenyl)diazenyl)phenyl)pyridine (TFAP) is synthesized with the following steps. 4-(Trifluoromethyl)aniline (400 mg, 2.48 mmol) were dissolved in CH_2Cl_2 (10 mL), a solution of Oxone (1.525 g, 4.96 mmol) in water (5 mL) was added. The mixture was stirred at room temperature overnight. After that, the organic phase was washed with brine (3 × 25 mL). The solvent was evaporated under vacuum, affording 1-nitroso-4-(trifluoromethyl)benzene as a greenish solid that was used without further purification. The crude was then suspended in acetic acid (20 mL), and 4-(pyridin-4-yl)aniline (337 mg, 1.98 mmol) was added, and the reaction was stirred at room temperature under inert atmosphere for 24 h. The crude was basified with KOH (6 M) and extracted with ethyl acetate (3 × 25 mL), and the combined organic phases were washed with brine (2 × 50 mL). The solvent was eliminated under vacuum, and the product was purified by column chromatography in hexane/ethyl acetate (10/6) obtaining the desired product as an orange powder (350 mg, 53%).

UV−vis Spectroscopy. UV−vis spectra in solution were recorded on JASCO V-670 spectrophotometer in 1 cm path quartz cuvettes. All the experiments were done using spectroscopic grade solvents. UV and visible light irradiation was done with an optical fiber-coupled LEDs (ThorLabs): for UV light, λ_{max} = 367 nm, FWHM = 9 nm; for vis light, λ_{max} = 451 nm, FWHM = 20 nm. UV−vis spectra on film are measured with CVD-grown monolayer triangle MX_2 film on double-polished sapphire (6carbon, China) without any further transfer process.

UPLC-HRMS Measurement. Chromatograms were recorded on a UPLC Ultimate3000 hyphenated to an HRMS (ESI+ Orbitrap) Executive Plus EMR system from Thermo Fisher Scientific. UPLC was run during 3.21 min using a gradient mode, starting with 98% of H_2O (0.05% formic acid) and 2% and CAN (0.05% formic acid) with an RP-C18 Hyper Gold Sil from Thermo Fisher at 1.15 mL min^{-1}. The quantification of the different isomers was done by integration of all the ionic species generated by each compound. The fraction of the corresponding isomer was calculated as the area of the isomer divided by the area of the sum of both components and was expressed in %.

Device Fabrication. All electronic devices were patterned by photolithography (AZ1505 photoresist and MIF726 developer, Micro Chemicals) using laser writer LW405B from Microtech. For MX_2 MOSFET, 60 nm of gold were thermally evaporated with Plassys MEB 300 followed by a lift-off process in warm acetone to obtain the final source and drain electrodes. For WSe_2 Schottky junctions, one electrode was first patterned with laser writer and 60 nm Pd was deposited; after lift-off in warm acetone, a second electrode was patterned followed by depositing 60 nm Ag with Egun evaporator Plassys ME300. For MX_2 inverter, the NMOS were first fabricated by patterning the electrode and depositing 60 nm Au. The PMOS were next fabricated through the deposition of 60 nm Pd as electrode metal. The devices were rinsed with acetone and 2-propanol to remove resist residues. All devices were annealed under vacuum at 100 °C to remove absorbents.

Electrical Characterizations. The characterization of device performance was realized by Keithley 2636A and 2635A under N_2 atmosphere. The *in situ* photoswitching is performed by a Polychrome V system (Thermo Fisher) used as a monochromatic light source. The output power has been calibrated by a PM100A Power Meter (Thorlabs) where the 365 nm UV light is 13.5 mW/cm^2 and 680 nm vis light is 15.5 mW/cm^2. All the electrical measurements were done in the dark to exclude the photoconductive effect of 2D materials.

The charge carrier density change Δn upon molecular doping of a semiconducting material, complying with the following equation:

$$\Delta n = \frac{C_{ox}\Delta V_{th}}{e} = \frac{\varepsilon_{ox}\Delta V_{th}}{t_{ox}e}$$

where Δn is the change in electron (negative charge) density, C_{ox} is the capacitance per unit area of 270 nm SiO_2, e is the elementary

https://doi.org/10.1021/acsnano.1c05167
ACS Nano 2021, 15, 13732−13741

charge, and ε_{ox} is the dielectric constant; ΔV_{th} is the change of the threshold voltage and t_{ox} is the thickness of dielectric.

Raman and Photoluminescence Spectroscopy. Raman and photoluminescence spectra were carried out by a Renishaw inVia spectrometer equipped with 532 nm laser. The excitation power was kept below 1 mW to avoid local heating damage effects. The wavenumber (energy) resolution was ∼1 meV.

AFM Measurement. AFM imaging was performed by means of a Bruker Dimension Icon setup operating in air, in tapping mode, by using tip model TESPA-V2 (tip stiffness: k = 42 N/m).

XPS Measurements. CVD-grown monolayer triangle MX_2 films on Si/SiO_2 (6carbon, China) were applied for XPS measurement without any further transfer process. XPS analyses were carried out with a Thermo Scientific K-Alpha X-ray photoelectron spectrometer with a basic chamber pressure of $\sim 10^{-9}$ mbar and an Al anode as the X-ray source (X-ray radiation of 1486 eV). Spot sizes of 400 μm and pass energies of 200.00 eV for wide energy scans and 10.00−20.00 eV for scans were used.

Computational Details. DFT calculations were performed using the VASP code[54] using the projector-augmented wave (PAW) basis set. Exchange and correlation effects are treated at the Perdew−Burke−Ernzerhof (PBE) level[55,56] with the dispersion forces included by Grimme correction (PBE+D2),[2,3] with a kinetic energy cutoff of 500 eV and using a Monkhorst−Pack sampling of 2 × 2 × 1 for the Brillouin zone (BZ) integration on the unit cell replicated 10 × 10 × 1 times with the vacuum spacing set to be 50 Å to avoid the interaction with periodic images. Dipole moment correction was employed along the c axis (Z direction and perpendicular to the TMDC surface). Geometries of MoS_2 and WSe_2 monolayers, as well as the Cis-CoPc(TFAP) and Trans-CoPc(TFAP) adsorbed heterostructures, were fully optimized at the PBE/GGA level of theory prior to the calculation of work function, using a Monkhorst−Pack sampling of 1 × 1 × 1 for the Brillouin zone (BZ) integration to minimize the computational cost. The work function (φ) of all the systems was calculated as the difference of Fermi energy (E_f, taken as the valence band maximum) and the electrostatic potential at vacuum level (E_p).

ASSOCIATED CONTENT

Supporting Information

The Supporting Information is available free of charge at https://pubs.acs.org/doi/10.1021/acsnano.1c05167.

Synthetic details, NMR spectra, DFT calculations, optical microscope images, surface characterizations (UV−vis spectroscopy, AFM, XPS), contrast experiments, and statistical analysis of the devices (PDF)

AUTHOR INFORMATION

Corresponding Author

Paolo Samorì − *University of Strasbourg,CNRS, ISIS UMR 7006, F-67000 Strasbourg, France;* orcid.org/0000-0001-6256-8281; Email: samori@unistra.fr

Authors

Ye Wang − *University of Strasbourg,CNRS, ISIS UMR 7006, F-67000 Strasbourg, France*

Daniel Iglesias − *University of Strasbourg,CNRS, ISIS UMR 7006, F-67000 Strasbourg, France*

Sai Manoj Gali − *Laboratory for Chemistry of Novel Materials, Université de Mons, 7000 Mons, Belgium;* orcid.org/0000-0002-0388-7888

David Beljonne − *Laboratory for Chemistry of Novel Materials, Université de Mons, 7000 Mons, Belgium;* orcid.org/0000-0002-2989-3557

Complete contact information is available at: https://pubs.acs.org/10.1021/acsnano.1c05167

Author Contributions

P.S and Y.W. conceived and coordinated the work. Y.W. worked on sample preparation, device fabrication, and optical and electrical characterization. D.I. synthesized and characterized the photochemistry of TFAP and CoPc(TFAP). Y.W. and D.I. analyzed the data. S.M.G. did the modeling work, under the supervision of D.B. Y.W. and P.S. wrote the paper with all the authors contributing to the discussion and preparation of the manuscript.

Funding

ERC project SUPRA2DMAT (GA-833707) Graphene Flagship Core 3 project (GA- 881603) Labex projects CSC (ANR-10-LABX-0026 CSC) Investissement d'Avenir program (ANR-10-120 IDEX-0002-02) NIE (ANR-11-LABX-0058 NIE) F.R.S.-FNRS under Grant 2.5020.11

Notes

The authors declare no competing financial interest.

ACKNOWLEDGMENTS

We acknowledge funding from European Commission through the ERC project SUPRA2DMAT (GA-833707), the Graphene Flagship Core 3 project (GA- 881603), the Agence Nationale de la Recherche through the Labex projects CSC (ANR-10-LABX-0026 CSC) and NIE (ANR-11-LABX-0058 NIE) within the Investissement d'Avenir program (ANR-10-120 IDEX-0002-02), the International Center for Frontier Research in Chemistry (icFRC) and the Institut Universitaire de France (IUF). The work in Mons is supported by the Belgian National Fund for Scientific Research (FRS-FNRS), within FNRS-PDR-TOREADOR project. Computational resources were provided by the Consortium des Équipements de Calcul Intensif (CÉCI) funded by F.R.S.-FNRS under Grant 2.5020.11. D.B. is FNRS Research Director. Device fabrication was carried out in part at the nanotechnology facility eFab (IPCMS, Strasbourg). The authors are grateful to H. Majjad, R. Bernard, and S. Siegwald for assistance with microfabrication.

REFERENCES

(1) Liu, C.; Chen, H.; Wang, S.; Liu, Q.; Jiang, Y.-G.; Zhang, D. W.; Liu, M.; Zhou, P. Two-Dimensional Materials for Next-Generation Computing Technologies. *Nat. Nanotechnol.* **2020**, *15* (7), 545−557.

(2) Waldrop, M. M. More Than Moore. *Nature* **2016**, *530* (7589), 144−147.

(3) Khan, H. N.; Hounshell, D. A.; Fuchs, E. R. Science and Research Policy at the End of Moore's Law. *Nat. Electron.* **2018**, *1* (1), 14−21.

(4) Migliato Marega, G.; Zhao, Y.; Avsar, A.; Wang, Z.; Tripathi, M.; Radenovic, A.; Kis, A. Logic-in-Memory Based on an Atomically Thin Semiconductor. *Nature* **2020**, *587* (7832), 72−77.

(5) Breyer, E. T.; Slesazeck, S. Ferroelectric Devices for Logic in Memory. *Ferroelectricity in Doped Hafnium Oxide: Materials, Properties and Devices*, 1st ed.; Woodhead Publishing Series in Electronic and Optical Materials; Woodhead Publishing: Cambridge, 2019; 495−513.

(6) Ashwell, G. J. Photochromic Memory Devices. *Nature* **1990**, *347* (6294), 617−617.

(7) Orgiu, E.; Samorì, P. 25th Anniversary Article: Organic Electronics Marries Photochromism: Generation of Multifunctional Interfaces, Materials, and Devices. *Adv. Mater.* **2014**, *26* (12), 1827−1845.

(8) Mosciatti, T.; Haar, S.; Liscio, F.; Ciesielski, A.; Orgiu, E.; Samorì, P. A Multifunctional Polymer-Graphene Thin-Film Transistor with Tunable Transport Regimes. *ACS Nano* **2015**, *9* (3), 2357−2367.

(9) Zhang, X.; Hou, L.; Samorì, P. Coupling Carbon Nanomaterials with Photochromic Molecules for the Generation of Optically Responsive Materials. *Nat. Commun.* **2016**, *7*, 11118.
(10) Leydecker, T.; Herder, M.; Pavlica, E.; Bratina, G.; Hecht, S.; Orgiu, E.; Samorì, P. Flexible Non-Volatile Optical Memory Thin-Film Transistor Device with Over 256 Distinct Levels Based on an Organic Bicomponent Blend. *Nat. Nanotechnol.* **2016**, *11* (9), 769−775.
(11) Zhao, Y.; Ippolito, S.; Samorì, P. Functionalization of 2D Materials with Photosensitive Molecules: From Light-Responsive Hybrid Systems to Multifunctional Devices. *Adv. Opt. Mater.* **2019**, *7* (16), 1900286.
(12) Crivillers, N.; Orgiu, E.; Reinders, F.; Mayor, M.; Samorì, P. Optical Modulation of the Charge Injection in an Organic Field-Effect Transistor Based on Photochromic Self-Assembled-Monolayer-Functionalized Electrodes. *Adv. Mater.* **2011**, *23* (12), 1447−1452.
(13) El Gemayel, M.; Börjesson, K.; Herder, M.; Duong, D. T.; Hutchison, J. A.; Ruzié, C.; Schweicher, G.; Salleo, A.; Geerts, Y.; Hecht, S.; Orgiu, E.; Samorì, P. Optically Switchable Transistors by Simple Incorporation of Photochromic Systems into Small-Molecule Semiconducting Matrices. *Nat. Commun.* **2015**, *6*, 6330.
(14) Orgiu, E.; Crivillers, N.; Herder, M.; Grubert, L.; Pätzel, M.; Frisch, J.; Pavlica, E.; Duong, D. T.; Bratina, G.; Salleo, A.; Hecht, S.; Samorì, P. Optically Switchable Transistor via Energy-Level Phototuning in a Bicomponent Organic Semiconductor. *Nat. Chem.* **2012**, *4* (8), 675.
(15) Carroli, M.; Dixon, A. G.; Herder, M.; Pavlica, E.; Hecht, S.; Bratina, G.; Orgiu, E.; Samorì, P. Multiresponsive Nonvolatile Memories Based on Optically Switchable Ferroelectric Organic Field-Effect Transistors. *Adv. Mater.* **2021**, *33*, 2007965.
(16) Qiu, H.; Liu, Z.; Yao, Y.; Herder, M.; Hecht, S.; Samorì, P. Simultaneous Optical Tuning of Hole and Electron Transport in Ambipolar WSe2 Interfaced with a Bicomponent Photochromic Layer: From High-Mobility Transistors to Flexible Multilevel Memories. *Adv. Mater.* **2020**, *32* (11), 1907903.
(17) Qiu, H.; Zhao, Y.; Liu, Z.; Herder, M.; Hecht, S.; Samorì, P. Modulating the Charge Transport in 2D Semiconductors via Energy-Level Phototuning. *Adv. Mater.* **2019**, *31* (39), 1903402.
(18) Lemme, M. C. Graphene and 2D Layer Devices for More Moore and More-than-Moore Applications. In *Beyond-CMOS Nanodevices 2*, Balestra, F., Ed.; ISTE Ltd, London, John Wiley & Sons Inc.; Hoboken, NJ, 2014; pp 97−116.
(19) Lembke, D.; Bertolazzi, S.; Kis, A. Single-Layer MoS_2 Electronics. *Acc. Chem. Res.* **2015**, *48*, 100−110.
(20) Wang, Y.; Slassi, A.; Cornil, J.; Beljonne, D.; Samorì, P. Tuning the Optical and Electrical Properties of Few-Layer Black Phosphorus via Physisorption of Small Solvent Molecules. *Small* **2019**, *15*, 1903432.
(21) Wang, Y.; Gali, S. M.; Slassi, A.; Beljonne, D.; Samorì, P. Collective Dipole-Dominated Doping of Monolayer MoS_2: Orientation and Magnitude Control via the Supramolecular Approach. *Adv. Funct. Mater.* **2020**, *30* (36), 2002846.
(22) Lu, J.; Lipatov, A.; Vorobeva, N. S.; Muratov, D. S.; Sinitskii, A. Photoswitchable Monolayer and Bilayer Graphene Devices Enabled by in Situ Covalent Functionalization. *Adv. Electron. Mater.* **2018**, *4* (8), 1800021.
(23) Tang, Z.; George, A.; Winter, A.; Kaiser, D.; Neumann, C.; Weimann, T.; Turchanin, A. Optically Triggered Control of the Charge Carrier Density in Chemically Functionalized Graphene Field Effect Transistors. *Chem. - Eur. J.* **2020**, *26* (29), 6473−6478.
(24) Feng, W.; Luo, W.; Feng, Y. Photo-Responsive Carbon Nanomaterials Functionalized by Azobenzene Moieties: Structures, Properties and Application. *Nanoscale* **2012**, *4* (20), 6118−6134.
(25) Döbbelin, M.; Ciesielski, A.; Haar, S.; Osella, S.; Bruna, M.; Minoia, A.; Grisanti, L.; Mosciatti, T.; Richard, F.; Prasetyanto, E. A.; De Cola, L.; Palermo, V.; Mazzaro, R.; Morandi, V.; Lazzaroni, R.; Ferrari, A. C.; Beljonne, D.; Samorì, P. Light-Enhanced Liquid-Phase Exfoliation and Current Photoswitching in Graphene−Azobenzene Composites. *Nat. Commun.* **2016**, *7*, 11090.
(26) Zhao, Y.; Bertolazzi, S.; Samorì, P. A Universal Approach toward Light-Responsive Two-Dimensional Electronics: Chemically Tailored Hybrid van der Waals Heterostructures. *ACS Nano* **2019**, *13* (4), 4814−4825.
(27) Li, J.; Wierzbowski, J.; Ceylan, Ö.; Klein, J.; Nisic, F.; Le Anh, T.; Meggendorfer, F.; Palma, C. A.; Dragonetti, C.; Barth, J. V.; Finley, J. J.; Margapoti, E. Tuning the Optical Emission of MoS_2 Nanosheets Using Proximal Photoswitchable Azobenzene Molecules. *Appl. Phys. Lett.* **2014**, *105* (24), 241116−241116.
(28) Baisch, B.; Raffa, D.; Jung, U.; Magnussen, O. M.; Nicolas, C.; Lacour, J.; Kubitschke, J.; Herges, R. Mounting Freestanding Molecular Functions onto Surfaces: the Platform Approach. *J. Am. Chem. Soc.* **2009**, *131* (2), 442−443.
(29) Zhang, Q.; Huang, Z.; Hou, Y.; Yuan, P.; Xu, Z.; Yang, H.; Song, X.; Chen, Y.; Yang, H.; Zhang, T. Tuning Molecular Superlattice by Charge-Density-Wave Patterns in Two-Dimensional Monolayer Crystals. *J. Phys. Chem. Lett.* **2021**, *12* (14), 3545−3551.
(30) Zhang, L.; Yang, T.; Zhang, W.; Qi, D.; He, X.; Xing, K.; Wong, P. K. J.; Feng, Y. P.; Wee, A. T. S. Bi-Stable Electronic States of Cobalt Phthalocyanine Molecules on Two-Dimensional Vanadium Diselenide. *Appl. Mater. Today* **2020**, *18*, 100535.
(31) Rusch, T. R.; Schlimm, A.; Krekiehn, N. R.; Tellkamp, T.; Budzák, Š.; Jacquemin, D.; Tuczek, F.; Herges, R.; Magnussen, O. M. Observation of Collective Photoswitching in Free-Standing TATA-Based Azobenzenes on Au (111). *Angew. Chem., Int. Ed.* **2020**, *59* (39), 17192−17196.
(32) Rusch, T. R.; Hammerich, M.; Herges, R.; Magnussen, O. M. Molecular Platforms as Versatile Building Blocks for Multifunctional Photoswitchable Surfaces. *Chem. Commun.* **2019**, *55* (64), 9511−9514.
(33) Brill, A. R.; Biswas, S.; Caspary Toroker, M.; de Ruiter, G.; Koren, E. Dipole-Induced Raman Enhancement Using Noncovalent Azobenzene-Functionalized Self-Assembled Monolayers on Graphene Terraces. *ACS Appl. Mater. Interfaces* **2021**, *13* (8), 10271−10278.
(34) Brill, A. R.; Kuntumalla, M. K.; de Ruiter, G.; Koren, E. Formation of Highly Ordered Self-Assembled Monolayers on Two-Dimensional Materials via Noncovalent Functionalization. *ACS Appl. Mater. Interfaces* **2020**, *12* (30), 33941−33949.
(35) Amsterdam, S. H.; Stanev, T. K.; Zhou, Q.; Lou, A. J.-T.; Bergeron, H.; Darancet, P.; Hersam, M. C.; Stern, N. P.; Marks, T. J. Electronic Coupling in Metallophthalocyanine−Transition Metal Dichalcogenide Mixed-Dimensional Heterojunctions. *ACS Nano* **2019**, *13* (4), 4183−4190.
(36) Choi, J.; Zhang, H.; Choi, J. H. Modulating Optoelectronic Properties of Two-Dimensional Transition Metal Dichalcogenide Semiconductors by Photoinduced Charge Transfer. *ACS Nano* **2016**, *10* (1), 1671−1680.
(37) Choudhury, P.; Ravavarapu, L.; Dekle, R.; Chowdhury, S. Modulating Electronic and Optical Properties of Monolayer MoS_2 Using Nonbonded Phthalocyanine Molecules. *J. Phys. Chem. C* **2017**, *121* (5), 2959−2967.
(38) Pak, J.; Jang, J.; Cho, K.; Kim, T.-Y.; Kim, J.-K.; Song, Y.; Hong, W.-K.; Min, M.; Lee, H.; Lee, T. Enhancement of Photodetection Characteristics of MoS_2 Field Effect Transistors Using Surface Treatment with Copper Phthalocyanine. *Nanoscale* **2015**, *7* (44), 18780−18788.
(39) Shankar, S.; Peters, M.; Steinborn, K.; Krahwinkel, B.; Sönnichsen, F. D.; Grote, D.; Sander, W.; Lohmiller, T.; Rüdiger, O.; Herges, R. Light-Controlled Switching of the Spin State of Iron (III). *Nat. Commun.* **2018**, *9*, 4750.
(40) Ludwig, J.; Moje, T.; Röhricht, F.; Herges, R. Synthesis of 4-Substituted Azopyridine-Functionalized Ni (II)-Porphyrins as Molecular Spin Switches. Beilstein. *Beilstein J. Org. Chem.* **2020**, *16* (1), 2589−2597.
(41) Otsuki, J.; Seki, E.; Taguchi, T.; Asakawa, M.; Miyake, K. STM Observation of Labile Axial Ligands to Zinc Porphyrin at Liquid/Solid Interface. *Chem. Lett.* **2007**, *36* (6), 740−741.
(42) Orbelli Biroli, A.; Calloni, A.; Bossi, A.; Jagadeesh, M. S.; Albani, G.; Duò, L.; Ciccacci, F.; Goldoni, A.; Verdini, A.; Schio, L.

https://doi.org/10.1021/acsnano.1c05167
ACS Nano 2021, 15, 13732−13741

Out-of-Plane Metal Coordination for a True Solvent-Free Building with Molecular Bricks: Dodging the Surface Ligand Effect for On-Surface Vacuum Self-Assembly. *Adv. Funct. Mater.* **2021**, *31*, 2011008.
(43) Rodríguez-Redondo, J. L.; Sastre-Santos, Á.; Fernández-Lázaro, F.; Soares, D.; Azzellini, G. C.; Elliott, B.; Echegoyen, L. Phthalocyanine-Modulated Isomerization Behaviour of an Azo-Based Photoswitch. *Chem. Commun.* **2006**, *12*, 1265−1267.
(44) Gao, Y.; Walter, V.; Ferguson, M. J.; Tykwinski, R. R. Hierarchical Synthesis, Structure, and Photophysical Properties of Gallium-and Ruthenium-Porphyrins with Axially Bonded Azo Ligands. *Chem. - Eur. J.* **2020**, *26*, 16712−16720.
(45) Reddy, D. R.; Maiya, B. G. A Molecular Photoswitch Based on an 'Axial-Bonding'Type Phosphorus (V) Porphyrin. *Chem. Commun.* **2001**, *1*, 117−118.
(46) Gobbi, M.; Bonacchi, S.; Lian, J. X.; Liu, Y.; Wang, X.-Y.; Stoeckel, M.-A.; Squillaci, M. A.; D'Avino, G.; Narita, A.; Müllen, K.; Feng, X.; Olivier, Y.; Beljonne, D.; Samorì, P.; Orgiu, E. Periodic Potentials in Hybrid van der Waals Heterostructures Formed by Supramolecular Lattices on Graphene. *Nat. Commun.* **2017**, *8*, 14767.
(47) Gobbi, M.; Bonacchi, S.; Lian, J. X.; Vercouter, A.; Bertolazzi, S.; Zyska, B.; Timpel, M.; Tatti, R.; Olivier, Y.; Hecht, S. Collective Molecular Switching in Hybrid Superlattices for Light-Modulated Two-Dimensional Electronics. *Nat. Commun.* **2018**, *9*, 2661.
(48) Gobbi, M.; Galanti, A.; Stoeckel, M.-A.; Zyska, B.; Bonacchi, S.; Hecht, S.; Samorì, P. Graphene Transistors for Real-Time Monitoring Molecular Self-Assembly Dynamics. *Nat. Commun.* **2020**, *11*, 4731.
(49) Li, J.; Wierzbowski, J.; Ceylan, Ö.; Klein, J.; Nisic, F.; Anh, T. L.; Meggendorfer, F.; Palma, C.-A.; Dragonetti, C.; Barth, J. V. Tuning the Optical Emission of MoS_2 Nanosheets Using Proximal Photoswitchable Azobenzene Molecules. *Appl. Phys. Lett.* **2014**, *105* (24), 241116.
(50) Kim, M.; Safron, N. S.; Huang, C.; Arnold, M. S.; Gopalan, P. Light-Driven Reversible Modulation of Doping in Graphene. *Nano Lett.* **2012**, *12* (1), 182−187.
(51) Zhang, M.; Yu, J.; He, J.; Huang, C. Adjusting Fermi Level of Graphene by Controlling the Linker Lengths of Dipolar Molecules. *Langmuir* **2019**, *35* (16), 5448−5454.
(52) Tran, M. D.; Kim, H.; Kim, J. S.; Doan, M. H.; Chau, T. K.; Vu, Q. A.; Kim, J. H.; Lee, Y. H. Two-Terminal Multibit Optical Memory via van der Waals Heterostructure. *Adv. Mater.* **2019**, *31* (7), 1807075.
(53) Lee, S.-J.; Lin, Z.; Huang, J.; Choi, C. S.; Chen, P.; Liu, Y.; Guo, J.; Jia, C.; Wang, Y.; Wang, L. Programmable Devices Based on Reversible Solid-State Doping of Two-Dimensional Semiconductors with Superionic Silver Iodide. *Nat. Electron.* **2020**, *3* (10), 630−637.
(54) Kresse, G.; Joubert, D. From Ultrasoft Pseudopotentials to the Projector Augmented-Wave Method. *Phys. Rev. B: Condens. Matter Mater. Phys.* **1999**, *59* (3), 1758.
(55) Perdew, J. P.; Burke, K.; Ernzerhof, M. Generalized Gradient Approximation Made Simple. *Phys. Rev. Lett.* **1996**, *77* (18), 3865.
(56) Grimme, S. Semiempirical GGA-Type Density Functional Constructed with a Long-Range Dispersion Correction. *J. Comput. Chem.* **2006**, *27* (15), 1787−1799.

https://doi.org/10.1021/acsnano.1c05167
ACS Nano 2021, 15, 13732−13741